PROCEEDINGS OF SCIENCE

Five texture zeros in the lepton sector that reproduce the observable neutrino masses and mixings: A mapping between the standard parameterization and our parameterization

Alejandro Rico,[a,*] **Richard H. Benavides,**[a] **D. V. Forero,**[b] **Luis Muñoz**[a] **and A. Tapia**[b]

[a] *Instituto Tecnológico Metropolitano, Facultad de Ciencias Exactas y Aplicadas*
Calle 73 N° 76-354 via el volador, Medellín, Colombia
[b] *Universidad de Medellín, Facultad de Ciencias Básicas,*
Cr 87 N° 30 - 65, Medellín, Colombia
E-mail: alejandromejia6237@correo.itm.edu.co, richardbenavides@itm.edu.co, dvanegas@udemedellin.edu.co, luismunoz@itm.edu.co, atapia@udemedellin.edu.co

In this work we have found analytical relations between the standard parameterization of the lepton mixing matrix (in the PDG convention) and the one obtained after considering five texture zeros in lepton mass matrices inspired by the Ramond-Robert-Ross forms originally applied to the quark sector. The particular lepton mass matrices structures were considered after assuming Dirac mass terms and a normal neutrino mass ordering. The lepton mixing matrices obtained are compatible with the neutrino oscillations phenomenology. To determine the analytical relation between the two parameterizations, a Taylor expansion up to second order was used such that the three mixing angles, and the Jarlskog invariant, are function of the free model parameters that come from the particular form of the chosen texture.

38th International Cosmic Ray Conference (ICRC2023)
26 July - 3 August, 2023
Nagoya, Japan

*Speaker

PoS(ICRC2023)1047

1. Introduction

Neutrino oscillations is the leading mechanism that successfully explains the flavor transitions observed in several experiments detecting neutrinos, from natural and artificial sources, using diverse experimental techniques, and for more than two decades [1]. It is therefore an experimental fact that neutrinos have non-zero masses and that they mix following a very different mixing pattern than the one for quarks [2]. There have been some attempts to model the neutrino mixing, for instance as a result of implementing flavor symmetries [3]. However, after the measurement of a non-zero reactor mixing angle this option have lost prediction power because corrections are needed to accommodate the current neutrino phenomenology. Another possibility is to assume the so call *texture zeros* in order to reduce the large number of degrees involved in the enlarged 'flavor problem', while producing a lepton mixing compatible with current data. In Ref. [4] it was shown that with five symmetric zeros, motivated by the Ramond-Roberts-Ross (RRR) forms (originally applied to the quark sector) [5], a lepton mixing pattern, compatible with the current phenomenology, was obtained. Three right-handed neutrinos were included to the standard model, generating Dirac masses for the neutrinos, and a normal neutrino mass ordering was assumed. This study was purely numerical without giving major details to the analytical relations between the free parameters in the forms and the usual parameters in the particle data group (PDG) parametrization of the lepton mixing, i.e, the three mixing angles and the Dirac phase encoding charge-parity (CP) violation in the lepton sector. In this letter, we are filling the gap providing approximate analytical expressions accounting for the mapping between both parametrizations. This expressions are validated by direct comparison with the numerical exact results. As an example, one of the four forms studied in Ref. [4] is considered here although the procedure can be applied to any of the forms, producing similar results.

2. The case of the RRR$_4$-Form

The mass matrices defining the RRR$_4$ form are shown in the Table 1, following Ref. [4]. The different parameters in the Table 1 are related to the corresponding eigenvalues (physical masses in each sector, neutral (n) and charged (l)), i.e. $M^{diag}_{(n,l)} = \text{Diag}\{m_{(1,e)}, -m_{(2,\mu)}, m_{(3,\tau)}\}$ [6, 7], where the neutrino masses are numbered while the lepton ones are labeled with the flavor in the subscript $l = e, \mu, \tau$. The mentioned relations can be obtained using a procedure with the following invariants [4, 5, 8, 9]:

$$\text{Det}\{M_{(n,l)}\} = \text{Det}\{M^{diag}_{(n,l)}\}, \quad \text{Tr}\{M_{(n,l)}\} = \text{Tr}\{M^{diag}_{(n,l)}\}, \quad \text{Tr}\{[M_{(n,l)}]^2\} = \text{Tr}\{[M^{diag}_{(n,l)}]^2\}. \tag{1}$$

From the invariants in Eq. (1) the following conditions must be satisfied:

$$\begin{aligned} c_n &= -a_n + m_1 - m_2 + m_3, & a_l &= m_e - m_\mu, \\ |b_n| &= \sqrt{m_1 m_2 m_3/(-a_n + m_1 - m_2 + m_3)}, & |b_l| &= m_\tau, \\ |d_n| &= \sqrt{\frac{(a_n - m_1 + m_2)(a_n - m_1 - m_3)(a_n + m_2 - m_3)}{-a_n + m_1 - m_2 + m_3}}, & |c_l| &= \sqrt{m_e m_\mu}, \end{aligned} \tag{2}$$

Form	M_n	M_l
RRR_4	$\begin{pmatrix} 0 & 0 & \lvert b_n\rvert\, e^{i\alpha_1} \\ 0 & c_n & \lvert d_n\rvert\, e^{i\alpha_2} \\ \lvert b_n\rvert\, e^{-i\alpha_1} & \lvert d_n\rvert\, e^{-i\alpha_2} & a_n \end{pmatrix}$	$\begin{pmatrix} 0 & \lvert b_l\rvert\, e^{i\beta_1} & 0 \\ \lvert b_l\rvert\, e^{-i\beta_1} & c_l & 0 \\ 0 & 0 & a_l \end{pmatrix}$

Table 1: RRR_4-Form with five texture zeros, inspired by the Ramond-Robert-Ross forms [4, 5]. Here M_n and M_l are the neutral and the charged mass matrices, respectively.

To ensure the parameters in Eq. (2) are real, the mathematical restriction $m_1 - m_2 < a_n < m_3 - m_2$ must be satisfied.

Following Ref. [4], the lepton mixing matrix is obtained from the multiplication of rotation matrices and a Φ phase matrix that is diagonal: $K = R_l \Phi R_n^T$; where R_l and R_n are orthogonal rotation matrices that diagonalize the charged (M_l) and neutral sector (M_n) masses, respectively. The Φ matrix is defined as $\Phi = \mathrm{Diag}(1, e^{-i(\alpha_1-\alpha_2+\beta_1)}, e^{i[(\alpha_1+\alpha_2)-(\beta_1+\beta_2)]}) = \mathrm{Diag}(1, e^{i\phi_1}, e^{i\phi_2})$.

Explicitly, the matrices that diagonalize the real mass matrices are:

$$R_n = \begin{pmatrix} \sqrt{\frac{m_2 m_3 (a_n+m_2-m_3)}{(m_1+m_2)(m_1-m_3)(-a_n+m_1-m_2+m_3)}} & -\sqrt{\frac{m_1(a_n-m_1+m_2)(-a_n+m_1+m_3)}{(m_1+m_2)(m_3-m_1)(-a_n+m_1-m_2+m_3)}} & \sqrt{\frac{m_1(a_n+m_2-m_3)}{(m_1+m_2)(m_1-m_3)}} \\ -\sqrt{\frac{m_1 m_3(-a_n+m_1+m_3)}{(m_1+m_2)(m_2+m_3)(-a_n+m_1-m_2+m_3)}} & -\sqrt{\frac{m_2(a_n-m_1+m_2)(a_n+m_2-m_3)}{(m_1+m_2)(m_2+m_3)(a_n-m_1+m_2-m_3)}} & \sqrt{\frac{m_2(-a_n+m_1+m_3)}{(m_1+m_2)(m_2+m_3)}} \\ \sqrt{\frac{m_1 m_2(a_n-m_1+m_2)}{(m_3-m_1)(m_2+m_3)(-a_n+m_1-m_2+m_3)}} & \sqrt{\frac{m_3(a_n-m_1-m_3)(a_n+m_2-m_3)}{(m_1-m_3)(m_2+m_3)(a_n-m_1+m_2-m_3)}} & \sqrt{\frac{m_3(a_n-m_1+m_2)}{(m_3-m_1)(m_2+m_3)}} \end{pmatrix}, \tag{3}$$

and,

$$R_l = \begin{pmatrix} \sqrt{\frac{m_\mu}{(m_e+m_\mu)}} & \sqrt{\frac{m_e}{(m_e+m_\mu)}} & 0 \\ -\sqrt{\frac{m_e}{(m_e+m_\mu)}} & \sqrt{\frac{m_\mu}{(m_e+m_\mu)}} & 0 \\ 0 & 0 & 1 \end{pmatrix}. \tag{4}$$

Notice that we have denoted the lepton mixing matrix as K to differentiate it from the PDG parametrization [2] although both unitary matrices account for the lepton mixing.

The three mixing angles from the PDG parametrization of the lepton mixing matrix are related to the parametrization K, as follows:

$$\begin{aligned} \tan\theta_{12} &= |K_{e,2}|/|K_{e,1}|, \\ \sin\theta_{13} &= |K_{e,3}|, \\ \tan\theta_{23} &= |K_{\mu,3}|/|K_{\tau,3}|, \end{aligned} \tag{5}$$

where the elements of the mixing matrix K depends on the model parameters after rotation of the real mass matrices from the RRR_4 form in Tab. 1.

Eq. (5) is the starting point to find the desired mapping betwen the lepton mixing in the PDG parametrization [2] and the one obtained from the assumed texture. For the numerical analyses, the charged lepton masses are fixed to the current central values reported in Ref. [2]. Assuming normal neutrino mass ordering, the active neutrino masses, obtained from the solar and atmospheric mass-squared differences (whose values are fixed to the best-point in Ref. [1]), are in terms of the unknown absolute neutrino mass scale m_0 taken here as the free parameter with an upper bound of $\sim$ 1eV at 95% of C.L. from direct searches [2].

3. Mapping

In the Table 2 we summarize the main results from the fit performed in Ref. [4] to each one of the parameters $\{m_0, a_n, \phi_1, \phi_2\}$ of the RRR$_4$-form defined in Table 1. The best fit point (bfp) and the one sigma allowed range for each parameter are shown. The value of χ^2 at the bfp ($\chi^2_{\rm min}$) is given in the caption for completeness.

Parameter	Best fit	1σ range
m_0 ($\times 10^{-3}$ eV)	3.2	[3.0, 3.3]
a_n ($\times 10^{-2}$ eV)	1.8	[1.7, 1.8]
ϕ_1 ($\times 10^{-1}$ rad)	0	$[-3.1, 3.1]$
ϕ_2(rad)	Independent	

Table 2: Best fit parameters (second column) and one sigma allowed range for 1 d.o.f (third column) for each of the parameters of the RRR$_4$ form (first column) obtained from a χ^2 minimization [4]. The χ^2 value at the minimum is $\chi^2_{\rm min.} = 1.3$.

After determining the best-fit point for each one of the parameters, a database was created where each parameter is varied within its one-sigma range. After that, the mixing angles $\sin^2\theta_{12}$, $\sin^2\theta_{13}$, $\sin^2\theta_{23}$ and in the Jarlskog invariant $J_{CP} = {\rm Im}\{K^*_{e,1}K^*_{\mu,3}K_{e,3}K_{\mu,1}\}$ [10], are calculated. Subsequently, data interpolation was performed and a Taylor expansion was applied. As a result of this expansion, mathematical expressions were obtained showing a dependency with each one of the model parameters.

The results from the Taylor expansions around the best-fit point in the RRR$_4$ form, to second-order, are obtained and are shown in Eq. (6), Eq. (7), Eq. (8), and Eq. (9):

$$\begin{aligned}
\sin^2\theta_{13} \;\approx\;& 7.1\times10^{-3} + 3.5\times10^{4}a_n{}^2m_1{}^2\phi_1^2 + 1.5\times10 a_n{}^2m_1{}^2\phi_1 - 6.0\times10^{4}a_n{}^2m_1{}^2 \\
+\;& 2.0\times10^{2}a_n{}^2m_1\phi_1^2 - 7.6\times10^{-2}a_n{}^2m_1\phi_1 + 7.1\times10^{3}a_n{}^2m_1 - 4.0\times10^{-1}a_n{}^2\phi_1^2 \\
+\;& 1.2\times10^{-4}a_n{}^2\phi_1 + 3.3a_n{}^2 + 9.6a_nm_1{}^2\phi_1^2 - 4.7\times10^{-1}a_nm_1{}^2\phi_1 + 4.4\times10^{3}a_nm_1{}^2 \\
-\;& 3.2\times10 a_nm_1\phi_1^2 + 1.7\times10^{-3}a_nm_1\phi_1 - 7.9a_nm_1 - 3.5\times10^{-2}a_n\phi_1^2 - 6.1\times10^{-6}a_n\phi_1 \\
-\;& 4.7\times10^{-2}a_n + 3.6\times10 m_1{}^2\phi_1^2 + 5.5\times10^{-3}m_1{}^2\phi_1 - 1\times10^{2}m_1{}^2 - 5.8\times10^{-1}m_1\phi_1^2 \\
-\;& 4.9\times10^{-5}m_1\phi_1 + 2.6m_1 - 1.3\times10^{-12}\phi_1, \qquad (6)
\end{aligned}$$

$$\begin{aligned}
\sin^2\theta_{12} \approx\ & 4.2\times10^{-2} + 2.4\times10 a_n + 2.6\times10 a_n^2 + 1\times10^2 m_1 - 5.2\times10 a_n m_1 + 3.4\times10^4 a_n^2 m_1 \\
& - 7.6\times10^3 m_1^2 + 7.7\times10^3 a_n m_1^2 - 2.2\times10^6 a_n^2 m_1^2 - 7.9\times10^{-7}\phi_1 + 4.2\times10^{-5} a_n\phi_1 \\
& - 1.6\times10^{-3} a_n^2\phi_1 + 2.1\times10^{-4} m_1\phi_1 - 3.8\times10^{-2} a_n m_1\phi_1 + 9.4\times10^{-1} a_n^2 m_1\phi_1 \\
& - 3.5\times10^{-2} m_1^2\phi_1 + 5.4 a_n m_1^2\phi_1 - 1.4\times10^2 a_n^2 m_1^2\phi_1 - 8.3\times10^{-3}\phi_1^2 - 2.4\times10^{-1} a_n\phi_1^2 \\
& - 2.4 a_n^2\phi_1^2 - 1.7 m_1\phi_1^2 - 1.3\times10^2 a_n m_1\phi_1^2 + 9.6\times10^2 8 a_n^2 m_1\phi_1^2 + 2.8\times10^2 m_1^2\phi_1^2 \\
& + 9.5\times10^3 a_n m_1^2\phi_1^2 - 1.7\times10^4 a_n^2 m_1^2\phi_1^2, \qquad (7)
\end{aligned}$$

$$\begin{aligned}
\sin^2\theta_{23} \approx\ & 8.5\times10^{-1} - 1.7\times10 a_n - 2.7 a_n^2 + 1.3\times10 m_1 - 2.6\times10^2 a_n m_1 - 7.3\times10^3 a_n^2 m_1 \\
& - 6.1\times10^2 m_1^2 + 1.6\times10^4 a_n m_1^2 - 1.4\times10^5 a_n^2 m_1^2 - 1.7\times10^{-5}\phi_1 + 1.9\times10^{-3} a_n\phi_1 \\
& - 5.5\times10^{-2} a_n^2\phi_1 + 1.1\times10^{-2} m_1\phi_1 - 1.2 a_n m_1\phi_1 + 3.5\times10 a_n^2 m_1\phi_1 - 1.7 m_1^2\phi_1 \\
& + 1.9\times10^2 a_n m_1^2\phi_1 - 5.5\times10^3 a_n^2 m_1^2\phi_1 + 1.8\times10^{-4}\phi_1^2 + 2.7\times10^{-2} a_n\phi_1^2 \\
& + 8.1\times10^{-1} a_n^2\phi_1^2 + 7.9\times10^{-2} m_1\phi_1^2 + 1.2\times10 a_n m_1\phi_1^2 + 5.7\times10^2 a_n^2 m_1\phi_1^2 \\
& - 1.4\times10 m_1^2\phi_1^2 + 2.8\times10^2 a_n m_1^2\phi_1^2 - 3.4\times10^4 a_n^2 m_1^2\phi_1^2, \qquad (8)
\end{aligned}$$

$$\begin{aligned}
J_{CP} \approx\ & 2.1\times10^{-11} - 2.4\times10^{-9} a_n + 7.0\times10^{-8} a_n^2 - 1.4\times10^{-8} m_1 + 1.6\times10^{-6} a_n m_1 \\
& - 4.5\times10^{-5} a_n^2 m_1 + 2.2\times10^{-6} m_1^2 - 2.5\times10^{-4} a_n m_1^2 + 7.0\times10^{-3} a_n^2 m_1^2 \\
& - 6.5\times10^{-3}\phi_1 - 7.1\times10^{-2} a_n\phi_1 + 5.2 a_n^2\phi_1 - 1.8 m_1\phi_1 - 6.0 a_n m_1\phi_1 + 2.3\times10^3 a_n^2 m_1\phi_1 \\
& + 1.9\times10^2 m_1^2\phi_1 + 3.4\times10^3 a_n m_1^2\phi_1 - 1.7\times10^5 a_n^2 m_1^2\phi_1 + 1.3\times10^{-8}\phi_1^2 \\
& - 1.1\times10^{-6} a_n\phi_1^2 + 3.1\times10^{-5} a_n^2\phi_1^2 - 5.8\times10^{-6} m_1\phi_1^2 + 7.6\times10^{-4} a_n m_1\phi_1^2 \\
& - 2.2\times10^{-2} a_n^2 m_1\phi_1^2 + 9.5\times10^{-4} m_1^2\phi_1^2 - 1.2\times10^{-1} a_n m_1^2\phi_1^2 + 3.4 a_n^2 m_1^2\phi_1^2, \qquad (9)
\end{aligned}$$

As it was discussed in Ref. [4], in the case of the RRR$_4$-form, it was found the observables in Eq.(5) are independent of the ϕ_2-phase. However, after performing the expansion in the mixing angle $\sin^2\theta_{23}$, the phase ϕ_2 emerged, as shown in appendices A. It is important to note that this term is spurious, just appearing due to the approximation made, and its contribution is nearly negligible in any case. This was tested by performing the plots of the mapping comparing with the exact numerical results. Taking as reference the exact numerical result, the results using the approximate expressions did not deviate beyond a 1% margin of relative error.

A second-order expansion was necessary in some cases because, during the crosscheck analysis, when fixing two out of the three free model parameters at their best-fit point values, and varying the remaining parameter around the one-sigma range, the mixing angles and the Jarlskog invariant better agreed with the numerical exact results when a quadratic term is included. In Fig. 1, the parameters a_n and m_0 were fixed at their best-fit values, while the parameter ϕ_1 was varied within its one-sigma range for each one of the three mixing angles $\sin^2\theta_{12}$, $\sin^2\theta_{13}$, and $\sin^2\theta_{23}$. The black line represents the exact numerical result while the green line corresponds to the results for the second-order expansion expressions.

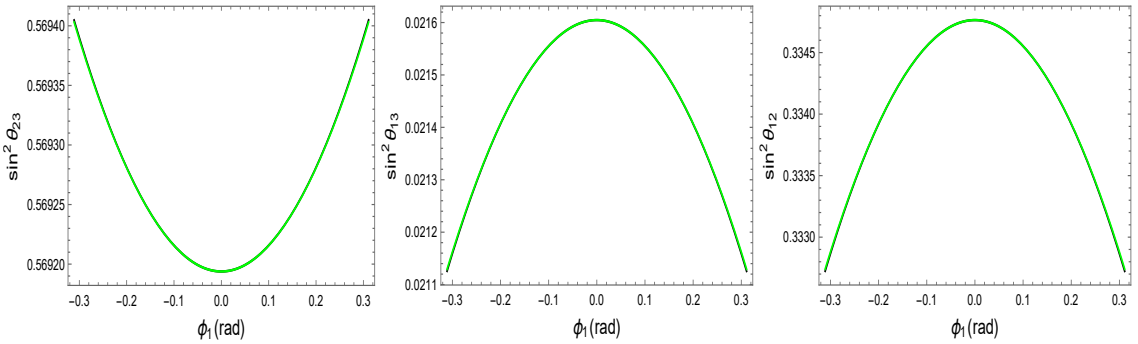

Figure 1: Mixing angles in terms of the ϕ_1-phase. The black line (under of green line) represents the exact numerical result, while the green line corresponds to the case when the second-order expansion expressions where used.

4. Analysis

Figures 2 and 3 show the correlation between two of the mixing angles, and the Jarlskog invariant and two of the mixing angles, respectively. The black dots correspond to the case when the exact numerical expressions where considered, while the green dots correspond to the results using the second-order expansion expressions varying randomly each one of the three model parameters $\{m_0, a_n, \phi_1\}$ within its one-sigma allowed range. Recall that for this particular form, the phase ϕ_2 is irrelevant. The numerical exact and the approximation expressions were evaluated 5000 times (points). It is worth noticing the excellent agreement between the exact and approximate cases.

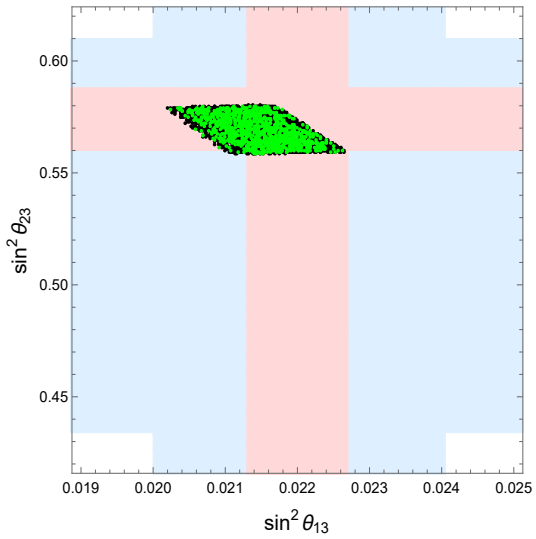

Figure 2: Correlation between the reactor mixing angle $\sin^2\theta_{13}$ and the atmospheric mixing angle $\sin^2\theta_{23}$. The broader vertical (horizontal) bands are the current allowed values for $\sin^2\theta_{13}$ ($\sin^2\theta_{23}$) at 3σ of C.L for 1 d.o.f. The thinner bands correspond to the preferred regions at 1σ of C.L for 1 d.o.f, following the results from the neutrino global-fit analysis in Ref. [1].

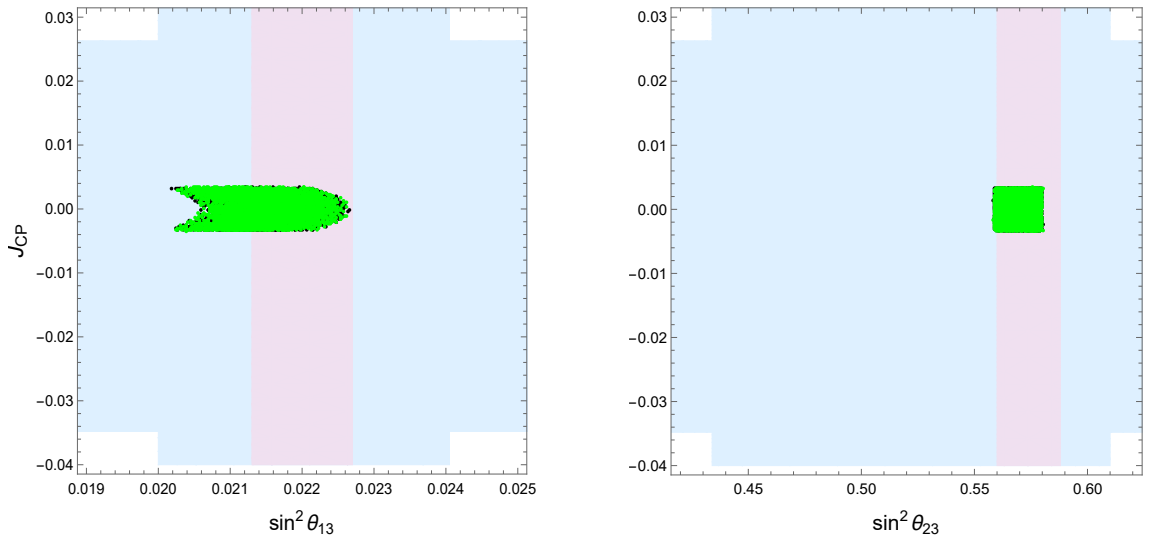

Figure 3: Correlation between the magnitude of the CP violation accounted by the Jarlskog invariant and the reactor mixing angle $\sin^2\theta_{13}$ (left panel) and the atmospheric mixing angle $\sin^2\theta_{23}$ (right panel). The broader horizontal (vertical) band corresponds to the current allowed values for Jarlskog ($\sin^2\theta_{13}$ and $\sin^2\theta_{23}$) at 3σ C.L for 1 d.o.f. The thinner vertical bands correspond to the 1σ of C.L for 1 d.o.f, following the results from the neutrino global-fit analysis in Ref. [1]

5. Conclusions

With the development of this work, it has been shown that the physical observables related to the phenomenon of neutrino oscillations are independent of the parameterizations of the mixing matrices in the lepton sector used for their description. With this result, it is evident that there are more options than the standard parameterization, which serve to explain some of the features shown in the so-called physics of flavor. These parameterizations must finally have a correlation, as it has been shown in this work using a Taylor expansion up to second order in the variable parameters of the proposed texture, which is one of the possible forms of textures with five zeros that reproduce all the physical observables in the lepton sector, when neutrinos are treated as Dirac particles and a normal neutrino mass ordering is assumed.

6. Acknowledgments

We would like to thank “Centro de laboratorios de investigación parque-i, y a la dirección de Investigaciones ITM, P20246 Project”. A. T. and D. V. F. also thank ‘Vicerrectoría de CyT—UdeMedellin’ for all the support during the development of this work.

A. Appendix: Complete expression to second order for the mixing angle $\sin^2\theta_{23}$.

For this particular mixing angle, there appears a dependence with the ϕ_2-phase, whose contribution is practically negligible to the mapping as it was numerically checked. As discussed in reference [4], in the case of the RRR_4-form, it was found the observables in Eq. (5) are independent of the ϕ_2-phase. We therefore conclude that the dependence with the ϕ_2-phase is due to the

approximation made since it is an spurious parameter. However, we present the full mathematical expression here as a matter of consistency with the expansion method employed:

$$
\begin{aligned}
\sin^2\theta_{23} \approx\ & 8.5\times10^{-1} - 1.7\times10 a_n - 2.7 a_n^2 + 1.3\times10 m_1 - 2.6\times10^2 a_n m_1 - 7.3\times10^3 a_n^2 m_1 \\
& - 6.1\times10^2 m_1^2 + 1.6\times10^4 a_n m_1^2 - 1.4\times10^5 a_n^2 m_1^2 - 1.7\times10^{-5}\phi_1 + 1.9\times10^{-3} a_n\phi_1 \\
& - 5.5\times10^{-2} a_n^2\phi_1 + 1.1\times10^{-2} m_1\phi_1 - 1.2 a_n m_1\phi_1 + 3.5\times10 a_n^2 m_1\phi_1 - 1.7 m_1^2\phi_1 \\
& + 1.9\times10^2 a_n m_1^2\phi_1 - 5.5\times10^3 a_n^2 m_1^2\phi_1 + 1.8\times10^{-4}\phi_1^2 + 2.7\times10^{-2} a_n\phi_1^2 \\
& + 8.1\times10^{-1} a_n^2\phi_1^2 + 7.9\times10^{-2} m_1\phi_1^2 + 1.2\times10 a_n m_1\phi_1^2 + 5.7\times10^2 a_n^2 m_1\phi_1^2 \\
& - 1.4\times10 m_1^2\phi_1^2 + 2.8\times10^2 a_n m_1^2\phi_1^2 - 3.4\times10^4 a_n^2 m_1^2\phi_1^2 - 4.2\times10^{-7}\phi_2 \\
& + 4.8\times10^{-5} a_n\phi_2 - 1.4\times10^{-3} a_n^2\phi_2 + 2.7\times10^{-4} m_1\phi_2 - 3.0\times10^{-2} a_n m_1\phi_2 \\
& + 8.6\times10^{-1} a_n^2 m_1\phi_2 - 4.2\times10^2 m_1^2\phi_2 + 4.8 a_n m_1^2\phi_2 - 1.4\times10^2 a_n^2 m_1^2\phi_2 \\
& + 6.9\times10^{-6}\phi_1\phi_2 - 7.9\times10^{-4} a_n\phi_1\phi_2 + 2.3\times10^{-2} a_n^2\phi_1\phi_2 - 4.4\times10^{-3} m_1\phi_1\phi_2 \\
& + 5.0\times10^{-1} a_n m_1\phi_1\phi_2 - 1.4\times10 a_n^2 m_1\phi_1\phi_2 + 6.9\times10^{-1} m_1^2\phi_1\phi_2 - 7.9\times10 a_n m_1^2\phi_1\phi_2 \\
& + 2.3\times10^3 a_n^2 m_1^2\phi_1\phi_2 + 2.3\times10^{-5}\phi_1^2\phi_2 - 2.6\times10^{-3} a_n\phi_1^2\phi_2 + 7.5\times10^{-2} a_n^2\phi_1^2\phi_2 \\
& - 1.4\times10^{-2} m_1\phi_1^2\phi_2 + 1.7 a_n m_1\phi_1^2\phi_2 - 4.8\times10 a_n^2 m_1\phi_1^2\phi_2 + 2.3 m_1^2\phi_1^2\phi_2 \\
& - 2.6\times10^2 a_n m_1^2\phi_1^2\phi_2 + 7.5\times10^3 a_n^2 m_1^2\phi_1^2\phi_2 .
\end{aligned}
$$

References

[1] P. F. de Salas, D. V. Forero, S. Gariazzo, P. Martínez-Miravé, O. Mena, C. A. Ternes, M. Tórtola, and J. W. F. Valle, JHEP **02**, 071 (2021), arXiv:2006.11237 [hep-ph] .

[2] P. A. Zyla et al. (Particle Data Group), PTEP **2020**, 083C01 (2020).

[3] S. Morisi and J. W. F. Valle, Fortsch. Phys. **61**, 466 (2013), arXiv:1206.6678 [hep-ph] .

[4] R. H. Benavides, D. Forero, L. Muñoz, J. M. Munoz, A. Rico, and A. Tapia, Physical Review D **107** (2023), 10.1103/physrevd.107.036008.

[5] P. Ramond, R. G. Roberts, and G. G. Ross, Nucl. Phys. B **406**, 19 (1993), arXiv:hep-ph/9303320 .

[6] G. C. Branco, D. Emmanuel-Costa, and R. Gonzalez Felipe, Phys. Lett. B **477**, 147 (2000), arXiv:hep-ph/9911418 .

[7] G. Ahuja, M. Gupta, M. Randhawa, and R. Verma, Phys. Rev. D **79**, 093006 (2009), arXiv:0904.4534 [hep-ph] .

[8] W. A. Ponce and R. H. Benavides, Eur. Phys. J. C **71**, 1641 (2011), arXiv:1104.5475 [hep-ph] .

[9] R. H. Benavides, Y. Giraldo, L. Muñoz, W. A. Ponce, and E. Rojas, J. Phys. G **47**, 115002 (2020), arXiv:2002.01864 [hep-ph] .

[10] C. Jarlskog, Phys. Rev. Lett. **55**, 1039 (1985).